In-Plane/Out-of-Plane Librations of a Tethered System in Elliptic Orbits

In-Plane/Out-of-Plane Librations of a Tethered System in Elliptical Orbits*1

By Noboru TAKEICHI,*2 M. C. NATORI*3 and Nobukatsu OKUIZUMI*3

Key Words: Tethered Systems, Elliptical Orbits, Atmospheric Drag

Abstract

In-plane/out-of-plane librations of a tethered system in elliptical orbits are investigated. It is aimed to clarify the fundamental characteristics of libration of the tethered system subjected to orbital motion and atmospheric drag. Periodic solutions and their stability of a simplified 3-DOF model are analyzed, in which in-plane/out-of-plane librations and longitudinal elongation of the tether are considered. It is shown that the librations become asymptotically stable or unstable because of atmospheric drag. The effects of system parameters on stability are analyzed, and it is shown that the property of longitudinal elongation of the tether determines the nature of stability, that is, asymptotically stable or unstable. It is also shown that the property of atmospheric drag determines only the degree of stability. Results of direct numerical simulations show the validity of the results of stability analyses. Physical interpretation of the phenomena is also clearly shown.

Nomenclature

A: cross sectional area of tether
C: damping constant
C_d: drag coefficient
E: Young's modulus
$\boldsymbol{F}$: atmospheric drag ($=(F_x, F_y, F_z)^T$)
S: equivalent drag area corresponding to both tether and subsatellite
V: relative velocity
e: orbital eccentricity
l_n: natural length of tether
m_s: mass of subsatellite
r: orbital altitude
r_{peri}: orbital altitude at perigee
r_E: Earth radius
x, y, z: position in the orbital coordinates
λ: stability parameter
μ: Earth gravitational constant
ν: true anomaly
Ω: Earth angular velocity
ρ: atmospheric density

Subscripts

o: initial conditions
p: periodic solutions

1. Introduction

Many applications of tethered systems have been proposed because large-scale space structure systems can easily be constructed. A tethered system with multisubsatellites has been proposed to observe the atmospheric region from 150 km to 500 km[1] (Fig. 1), where balloons, aircraft, or single-body satellites cannot explore for a long duration. Because this system aims to observe the atmosphere, its orbital speed is reduced by atmospheric drag; therefore it is necessary to take a high-energy orbit. Since the observation altitude is limited, the system should take an elliptic orbit. Thus the tethered system is subjected to various changes of gravity-gradient and atmospheric environment.

In the author's recent study on this tethered system,[2] divergence of libration resulting from atmospheric drag has been observed in numerical simulations by use of a practical model, in which elasticity, lack of bending rigidity, distributed mass of the tether, and atmospheric drag on it are considered. It has been concluded that some improvements or active controls are necessary to execute a long-term observation. In this study, therefore, we aim to clarify the cause of divergence and the effects of system parameters on the stability of libration through the investigation of fundamental characteristics of the tethered system, which faces atmospheric drag in elliptical orbits.

In the previous studies on the dynamics of tethered systems in elliptical orbits, periodic solutions and chaotic motions are focused. The periodic solutions and the possibility of libration of in-plane motion of arbitrarily shaped satellites have been analyzed[3,4] to learn the critical eccentricity, beyond which libration is impossible. And it was shown that the libration of the most gravity-gradient-stabilized satellite is possible in elliptical orbits of $e<0.353$. In the study cited above, when the moment of inertia ratio is equal to 1, the satellite can be considered as a "longitudinally rigid" tethered system. On chaotic motions of tethered systems, numerical methods such as Poincare maps, bifurca-

*1 22nd International Symposium on Space Technology and Science, Morioka, Japan, May 28-June 4, 2000. Received June 14th, 2000.

*2 Department of Aeronautics and Astronautics, Graduate School of Engineering, the University of Tokyo, Tokyo, Japan.
*3 The Institute of Space and Astronautical Science, Sagamihara, Japan.

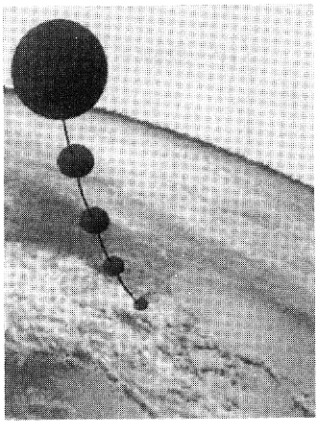

Fig. 1. Image of a tethered system for atmospheric observation.

tion diagrams and Lyapunov exponents have been applied to the nonlinear equations of motion.[5-8] And the motions of tethered systems were classified into quasi-periodic/periodic and chaotic motion, that is, libration and tumbling. The stability of the libration of tethered systems in circular and slightly eccentric orbits subjected to atmospheric drag has been investigated,[9-12] and it is shown that the equilibrium state can be unstable because of the combined effect of tether elasticity and atmospheric density gradient.

In this study, the gradual change of the libration, that is, divergence or convergence, is focused, and its stability is analyzed. Tethered systems in elliptic orbits face periodic disturbances of orbital motion and atmospheric drag. Therefore the systems can be regarded as periodic systems of one orbital period, and the stability of these periodic systems can be analyzed through the stability of periodic solutions of their equations of motion. The shooting method[13] is applied to investigate the periodic solutions and their stability, that is, whether they are asymptotically stable, stable, or unstable. As is known in the previous studies,[9-12] longitudinal elasticity of the tether is a significant factor in the investigation of stability of libration subjected to atmospheric drag. Futhermore, because the orbital eccentricity of the tethered system under investigation is relatively large, the equations of motion cannot be linearized. Therefore a 3-DOF model, which includes in-plane/out-of-plane librations and longitudinal elongation of the tether, is used, and its nonlinear equations of motion are investigated numerically.

2. Formulation

2.1. System configurations and assumptions The tethered system under consideration is shown in Fig. 2. Assumptions are made as follows:

- The orbital motion is decoupled with the attitude motion of the tethered system.
- The center of mass is moving in an equatorial orbit around the spherical earth.
- The subsatellite is connected by an elastic tether to the mother satellite, which coincides with the origin of the orbital coordinate.
- The mass and the bending rigidity of the tether are negligible.
- The spring constant and the damping coefficient are proportional to the cross-sectional area of the tether and inversely proportional to its length.
- Initially the tether is fully deployed, and active control of the tethered system is not considered.
- The atmospheric drag on both tether and subsatellite is assumed to concentrate on the subsatellite.
- The atmosphere rotates with the Earth, and its density is a function of only altitude.
- To focus on the libration of the tethered system, the orbital perturbation as a result of the atmospheric drag is not considered.

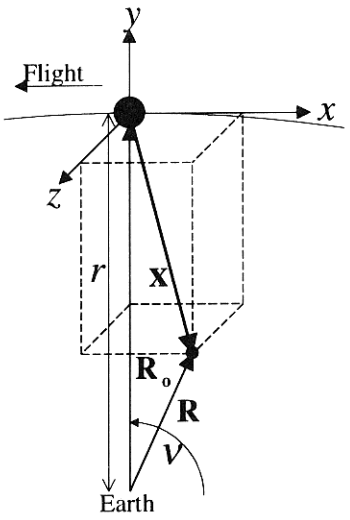

Fig. 2. Coordinates of a tethered system.

Through this model, in-plane/out-of-plane librations subjected to various changes of gravity-gradient, orbital angular velocity and atmospheric drag can be investigated.

2.2. Equations of motion Equations of motion are obtained through the Lagrange formulation. Let $\boldsymbol{x}$ and $\boldsymbol{R}$ be the position vector of the subsatellite in the orbital frame and in the inertial frame respectively, and let $\boldsymbol{R}_0$ be the position vector of the mothersatellite (Fig. 2). The following equations about their time differentials are obtained.

$$\boldsymbol{R}=\boldsymbol{R}_0+\boldsymbol{x} \qquad \ldots\ldots(1)$$

$$\dot{\boldsymbol{R}}=\dot{\boldsymbol{R}}_0+\dot{\boldsymbol{x}}+\dot{\boldsymbol{\nu}}\times(\boldsymbol{R}_0+\boldsymbol{x})$$

$$=\begin{Bmatrix}\dot{x}-\dot{\nu}(y+r)\\ \dot{y}+\dot{r}+\dot{\nu}x\\ \dot{z}\end{Bmatrix} \qquad \ldots\ldots(2)$$

The kinetic energy K and potential energy U can be expressed as follows:

$$K=\frac{1}{2}m_s|\dot{\boldsymbol{R}}|^2$$
$$=\frac{1}{2}m_s[\dot{x}^2+(\dot{y}+\dot{r})^2+\dot{z}^2+\dot{\nu}^2\{x^2+(y+r)^2\}$$
$$+2\dot{\nu}\{\dot{x}(y+r)+x(\dot{y}+\dot{r})\}] \quad \ldots.(3)$$

$$U=-\mu\frac{m_s}{|\boldsymbol{R}|}=-\mu m_s\{x^2+(y+r)^2+z^2\}^{-1/2} \quad \ldots.(4)$$

The elastic potential energy P and dissipation function W of the tether are expressed as

$$P=\frac{1}{2}\frac{EA}{l_n}(l-l_n)^2 \quad \ldots.(5)$$

$$W=\frac{1}{2}\frac{CA}{l_n}i^2 \quad \ldots.(6)$$

where,

$$l=|\boldsymbol{x}| \quad \ldots.(7)$$

Lagrangian L for the subsatellite is obtained as

$$L=K-U-P \quad \ldots.(8)$$

and the Lagrange equations of motion can be obtained as follows:

$$\frac{d}{dt}\left(\frac{\partial\sum L}{\partial\dot{q}}\right)-\frac{\partial\sum L}{\partial q}+\frac{\partial\sum W}{\partial\dot{q}}=Q \quad \ldots.(9)$$

We obtain the following equations of motion without approximation.

$$\ddot{x}=\ddot{\nu}(y+r)+x\dot{\nu}^2+2\dot{\nu}(\dot{y}+\dot{r})$$
$$-\mu x\{x^2+(y+r)^2+z^2\}^{-3/2}$$
$$-\frac{x}{m_s l}\left\{\frac{EA}{l_n}(l-l_n)+\frac{CA}{l_n}i\right\}+\frac{F_x}{m_s} \quad \ldots.(10)$$

$$\ddot{y}=-\ddot{r}-\ddot{\nu}x-2\dot{\nu}\dot{x}+(y+r)\nu^2$$
$$-\mu(y+r)\{x^2+(y+r)^2+z^2\}^{-3/2}$$
$$-\frac{y}{m_s l}\left\{\frac{EA}{l_n}(l-l_n)+\frac{CA}{l_n}i\right\}+\frac{F_y}{m_s} \quad \ldots.(11)$$

$$\ddot{z}=-\mu z\{x^2+(y+r)^2+z^2\}^{-3/2}$$
$$-\frac{z}{m_s l}\left\{\frac{EA}{l_n}(l-l_n)+\frac{CA}{l_n}i\right\}+\frac{F_z}{m_s} \quad \ldots.(12)$$

$\boldsymbol{F}$ is the vector of the atmospheric drag. The values of atmospheric drag on the tether and satellites are as follows:

$$\boldsymbol{F}=\frac{1}{2}\rho_{(r,y)}C_d S|\boldsymbol{V}|\boldsymbol{V} \quad \ldots.(13)$$

where,

$$\boldsymbol{V}=\begin{pmatrix}(\dot{\nu}-\Omega)(r+y)-\dot{x}\\-\dot{y}-\dot{r}\\-\dot{z}\end{pmatrix} \quad \ldots.(14)$$

Based on the assumptions, the equations of orbital motion is obtained as follows:

$$\ddot{r}=r\dot{\nu}^2-\frac{\mu}{r^2} \quad \ldots.(15)$$

$$\ddot{\nu}=-\frac{2\dot{\nu}\dot{r}}{r} \quad \ldots.(16)$$

Initial orbital parameters at the apogee are given as follows:

$$r_o=\frac{1+e}{1-e}(r_E+r_{peri}),\qquad \dot{r}_o=0,$$
$$\nu_o=0,\qquad \dot{\nu}_o=\sqrt{\frac{(1-e)\mu}{r_o^3}}. \quad \ldots.(17)$$

3. Numerical Methods

3.1. Shooting method To analyze the periodic solutions and their stability, the shooting method is applied to Eqs. (10)–(12).

The algorithm of the shooting method is as follows:

Define $\boldsymbol{x}$ as follows:

$$\boldsymbol{x}=(\dot{x},x,\dot{y},y,\dot{z},z)^T \quad \ldots.(18)$$

and Eqs. (10)–(12) can be written:

$$\frac{d}{dt}\boldsymbol{x}=\boldsymbol{X}(t,\boldsymbol{x}) \quad \ldots.(19)$$

Define $\boldsymbol{\psi}(t,\boldsymbol{\psi}_o)$ as the solution matrix of the following differential equation (20) of the initial condition $\boldsymbol{\psi}_o$.

$$\frac{d}{dt}\boldsymbol{\psi}=\boldsymbol{Y}(\boldsymbol{x})\boldsymbol{\psi} \quad \ldots.(20)$$

where, $\boldsymbol{Y}$ is the Jacobian matrix of $\boldsymbol{X}$ about $\boldsymbol{x}$.

$$\boldsymbol{Y}=\frac{\partial\boldsymbol{X}}{\partial\boldsymbol{x}} \quad \ldots.(21)$$

Integrate (19) and (20) for one orbital period T with the initial conditions $\boldsymbol{x}=\boldsymbol{x}_o$ and $\boldsymbol{\psi}=\boldsymbol{I}$. After integration, the correction vector $\delta\boldsymbol{x}$ can be obtained from the following equation (22):

$$[\boldsymbol{\psi}(T,\boldsymbol{I})-\boldsymbol{I}]\delta\boldsymbol{x}=\boldsymbol{x}_o-\boldsymbol{x}(T,\boldsymbol{x}_o) \quad \ldots.(22)$$

From the following equation (23), $\boldsymbol{x}_o^+$ can be obtained as the new initial condition.

$$\boldsymbol{x}_o^+=\boldsymbol{x}_o+\delta\boldsymbol{x} \quad \ldots.(23)$$

By iterating this procedure until $\delta\boldsymbol{x}$ becomes small

enough to satisfy the desired accuracy, the initial condition that leads to the periodic motion can be obtained as the final $\boldsymbol{x}_0^+$. And the stability is analyzed through λ, which is defined as the maximum absolute value of the eigenvalues of $\boldsymbol{\psi}(T, \boldsymbol{I})$.

From λ, the stability is verified as follows:

$\lambda=1$: Stable,

$\lambda>1$: Unstable, —Divergence,

$\lambda<1$: Asymptotically Stable, —Convergence,

and $\lambda-1$ mean the rapidity of convergence or divergence.

In this study, periodic solutions of the same period as one orbital revolution are analyzed, and the significant digit of the results of the shooting method is set at six.

3.2. Poincare maps A Poincare map consists of discrete plots created by sampling the values of states periodically, and it facilitates the understanding of the motion characteristics of a system by eliminating the information of time. In this paper, $(x, \dot{x})$ and $(z, \dot{z})$ are mapped at every apogee.

4. Numerical Analysis

4.1. System parameters The constant parameters are given as follows:

$$r_E=6378 \text{ [km]}, \quad \mu=3.986\times10^{14} \text{ [m}^3/\text{s}^2\text{]},$$
$$E=5.0\times10^9 \text{ [N/m}^2\text{]}, \quad C=2.0\times10^9 \text{ [Ns/m}^2\text{]}.$$

And values of the other parameters, such as r_{peri}, e, m_s, C_dS, l_n, and A, are given at every analysis.

The function of atmospheric density is given in the following equation, which is approximated for the range from 100 km to 500 km from the chart of Standard Atmosphere.[14] For a range higher than 500 km, the density is regarded as negligible.

$$\rho_{(h)}=\exp(-2.71\times10^{-2}h-15.8) \text{ [kg/m}^3\text{]} \quad \ldots\ldots (24)$$

where, h [km] is the altitude from Earth.

4.2. Periodic solutions Periodic solutions and their stability are analyzed by using the following parameters:

$$r_{peri}=250 \text{ [km]}, \quad e=0.2, \quad l_n=100 \text{ [km]},$$
$$m_s=100 \text{ [kg]}, \quad A=1.5\times10^{-6} \text{ [m}^2\text{]}, \quad C_dS=40 \text{ [m}^2\text{]}.$$

As a result, three periodic solutions are found; one is an in-plane solution and the other two are out-of-plane solutions, which are symmetrical to each other about the orbital plane. Figure 3 shows the motion of one of the out-of-plane solutions, and the out-of-plane trajectory of the other out-of-plane solution is symmetrical about the horizontal axis. The stability parameters of the in-plane and out-of-plane solutions are different, $\lambda-1=-7.2\times10^{-4}$ for the out-of-plane solutions and $\lambda-1=-5.8\times10^{-4}$ for the in-plane solution.

4.3. Effects of system parameters on stability In this section, the stability criteria and the effects of the system parameters on stability are analyzed through the shooting method. The following values are used as the standard set of parameters:

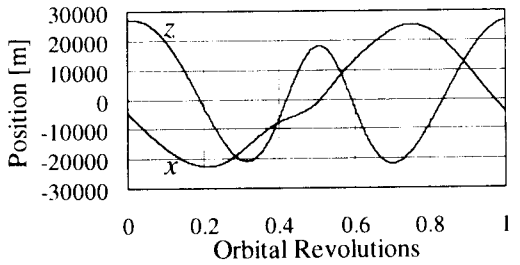

Fig. 3. Motion of periodic solution: Out-of-Plane: $m_s=100$ [kg], $e=0.2$.

$$e=0.2, \quad l_n=100 \text{ [km]}, \quad m_s=100 \text{ [kg]},$$
$$A=1.5\times10^{-6} \text{ [m}^2\text{]}, \quad C_dS=40 \text{ [m}^2\text{]},$$
$$r_{peri}=l_n+150 \text{ [km]},$$

and the periodic solutions are analyzed by letting one of these parameters vary individually. In all analyses, one in-plane solution and two out-of-plane solutions are always obtained. In this section, the smallest λ of the solutions are discussed in all cases. The results are shown in Fig. 4, and in the figures, the circle marks correspond to the case of $m_s=100$ [kg] and the cross marks correspond to the case of $m_s=500$ [kg]. Figure 4 (a) shows the result investigated about the eccentricity. This figure means that the critical eccentricities, beyond which any initial conditions do not lead the tethered system to continue libration, are $e\geq0.36$ for $m_s=100$ [kg], and $e\geq0.33$ for $m_s=500$ [kg]. It is suggested that the critical eccentricity diminishes as the mass of the subsatellite becomes larger. From Figs. 4 (b)–(d), it can be concluded that the larger mass of the subsatellite, the smaller cross-sectional area, and the longer tether decrease stability more, and after threshold values, the system becomes unstable. Therefore easy-to-elongate tethered systems tend to be unstable. Figures 4 (e) and (f) show that the librations of the system of $m_s=500$ [kg] are always unstable; those of the system of $m_s=100$ [kg] are always asymptotically stable; and $|\lambda-1|$ increases as the atmospheric drag increases. Therefore it is considered that drag coefficient, drag area, and perigee altitude do not determine whether the libration is asymptotically stable or unstable, but how rapidly the libration converges or diverges. In the case of $C_dS=0$ [m^2], the atmospheric drag is negligible, $\lambda-1\equiv0$ in both $m_s=100$ [kg] and $m_s=500$ [kg]. Therefore it can be concluded that the atmospheric drag stabilizes or destabilizes the libration as shown in Fig. 4 (f). In Fig. 4 (g), which is a vertically expanded figure of (a), the stability or instability increases as the eccentricity diminishes because the tethered system faces atmospheric drag for longer durations in the orbits of smaller eccentricity.

4.4. Dynamic behavior of libration In this section, dynamic behavior of the libration is investigated through

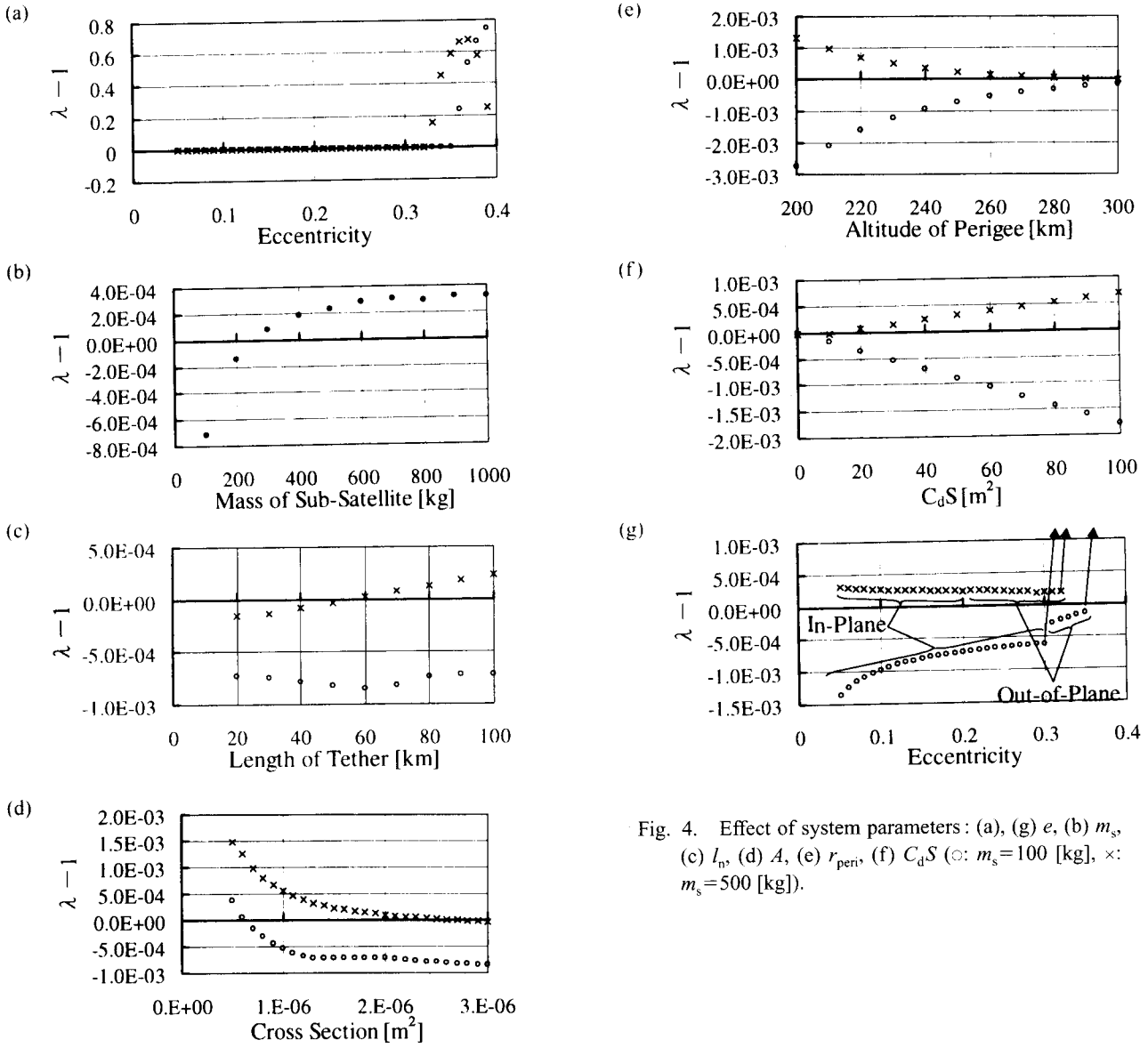

Fig. 4. Effect of system parameters: (a), (g) e, (b) m_s, (c) l_n, (d) A, (e) r_{peri}, (f) C_dS (○: m_s=100 [kg], ×: m_s=500 [kg]).

numerical integrations, and they are performed for 2,000 orbital revolutions in all cases. In the integrations, the same parameters as those used in the shooting method are given:

$$r_{peri}=250 \text{ [km]}, \quad e=0.2, \quad l_n=100 \text{ [km]},$$
$$m_s=100 \text{ [kg]} \text{ or } m_s=500 \text{ [kg]},$$
$$A=1.5\times10^{-6} \text{ [m}^2\text{]}, \quad C_dS=40 \text{ [m}^2\text{]}.$$

The stability parameters obtained from the shooting method are $\lambda-1=-7.2\times10^{-4}$ (asymptotically stable) for $m_s=100$ [kg] and $\lambda-1=2.3\times10^{-4}$ (unstable) for $m_s=500$ [kg]. Some sets of initial conditions leading the tethered system to librations, which are in the neighboring regions of the periodic solutions, are given in all cases. Figures 5 and 6 are typical numerical results of $m_s=100$ [kg]. The upper figures are Poincare maps of in-plane and out-of-plane motions, in which cross marks denote the states of in-plane periodic solutions, and circle marks denote those of the out-of-plane solutions. And the bottom figure shows a time history of the positions. In these figures, it can be seen that the libration converges on one of the stable periodic solutions. Figure 7 is the result of $m_s=500$ [kg]. In this case, the in-plane libration diverges from the periodic solution, and the out-of-plane libration converges. Therefore it is considered that atmospheric drag destabilizes only the in-plane libration. The tethered system should go slack and begin tumbling in the later duration.

5. Physical Interpretation

Let θ be the pitch angle of the tethered system, and the angular velocity of libration in the inertial coordinate is expressed as $\dot{v}+\dot{\theta}$. The centrifugal force of the tether is almost proportional to $(\dot{v}+\dot{\theta})^2$. When the backward swing is faster than that of the periodic solution around the perigee, the centrifugal force of the tether becomes larger than that of the periodic solution, the tether elongates, and the atmospheric density becomes larger ($\rho>\rho_p$). On the other hand, the relative velocity becomes smaller ($|V|<|V_p|$). In an easy-to-elongate tethered system, the following relation can

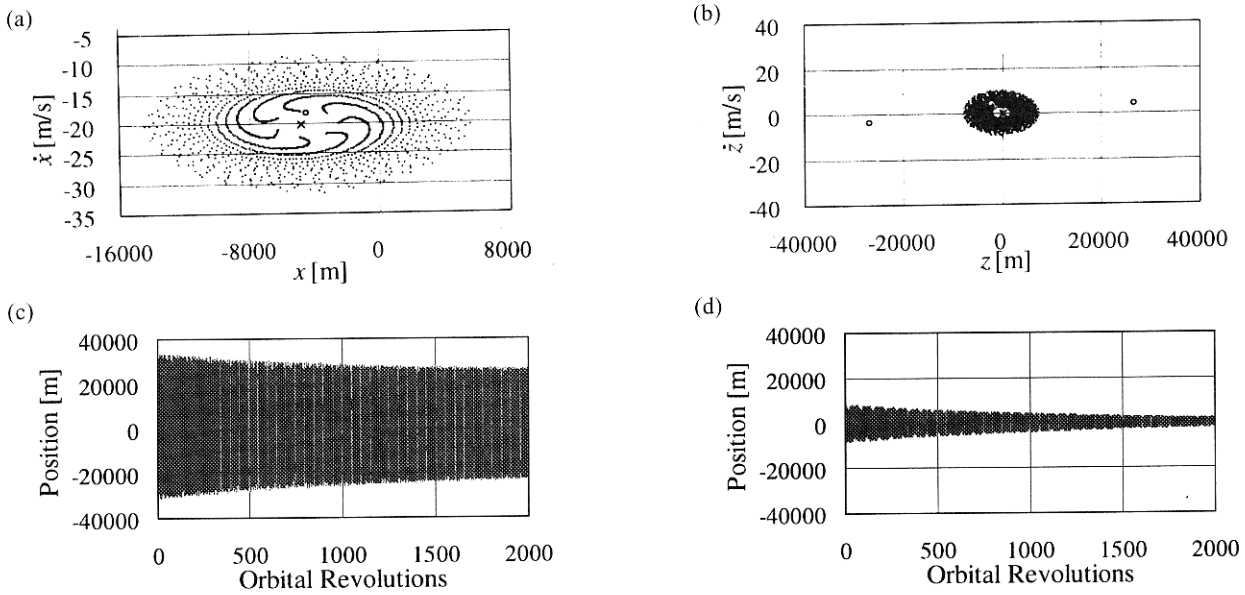

Fig. 5. Libration : m_s=100 [kg], Initial Conditions : $(x_o, \dot{x}_o)=(0, -10)$, $(z_o, \dot{z}_o)=(0, -10)$, (a) In-Plane Poincare map, (b) Out-of-Plane Poincare map, (c) In-Plane Time History, (d) Out-of-Plane Time History.

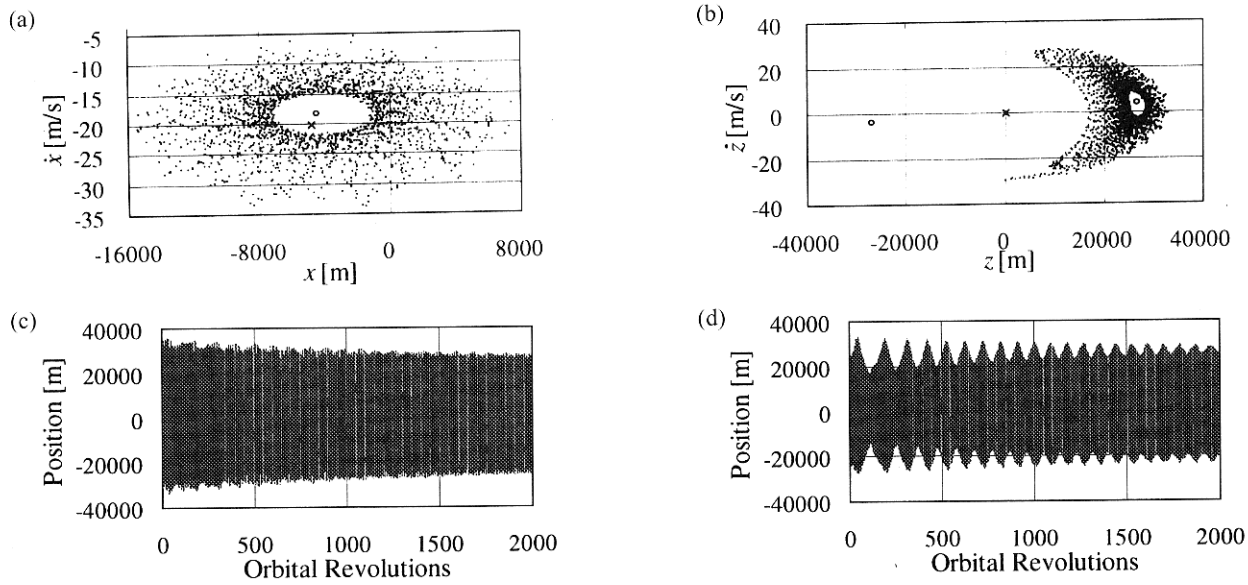

Fig. 6. Libration : m_s=500 [kg], Initial Conditions : $(x_o, \dot{x}_o)=(0, -10)$, $(z_o, \dot{z}_o)=(0, -30)$, (a) In-Plane Poincare map, (b) Out-of-Plane Poincare map, (c) In-Plane Time-History, (d) Out-of-Plane Time-History.

be valid :

$$\frac{\rho}{\rho_p} > \frac{|V_p|^2}{|V|^2} \quad \ldots\ldots (25)$$

then we obtain

$$|F| = \frac{1}{2} C_d S \rho |V|^2 > \frac{1}{2} C_d S \rho_p |V_p|^2 = |F_p| \quad \ldots\ldots (26)$$

From Eq. (26), it is considered that the backward swing of the system is accelerated by atmospheric drag, and the deviation from the periodic solution becomes larger. Inversely, the following equations (27) and (28) are valid in a hard-to-elongate tethered system, which means an opposite to easy-to-elongate tethered system ; the backward swing is decelerated, and the deviation becomes smaller.

$$\frac{\rho}{\rho_p} < \frac{|V_p|^2}{|V|^2} \quad \ldots\ldots (27)$$

$$|F| = \frac{1}{2} C_d S \rho |V|^2 < \frac{1}{2} C_d S \rho_p |V_p|^2 = |F_p| \quad \ldots\ldots (28)$$

When the backward swing is slower than that of the periodic solution, the atmospheric density is smaller and the relative velocity is larger. Therefore the following relation can be valid for an easy-to-elongate tethered system :

$$|F| < |F_p| \quad \ldots\ldots (29)$$

and for a hard-to-elongate tethered system :

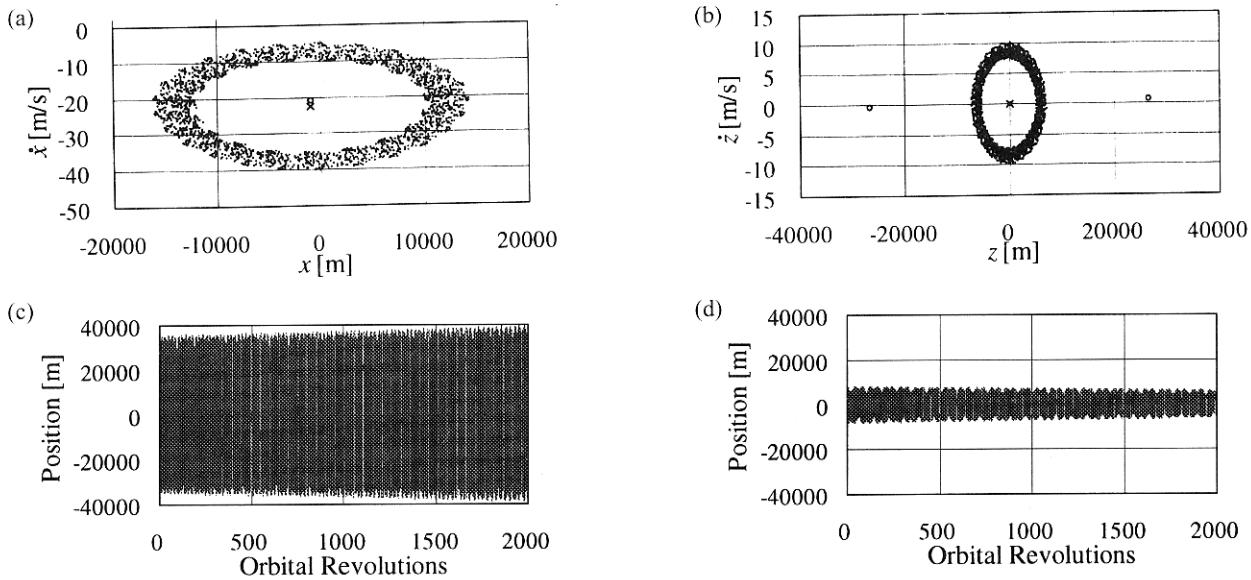

Fig. 7. Libration : m_s=500 [kg], Initial Conditions : $(x_o, \dot{x}_o)=(0, -10)$, $(z_o, \dot{z}_o)=(0, -10)$, (a) In-Plane Poincare map, (b) Out-of-Plane Poincare map, (c) In-Plane Time History, (d) Out-of-Plane Time History.

$$|\boldsymbol{F}| > |\boldsymbol{F}_p| \quad \ldots\ldots (30)$$

And the deviation becomes larger in an easy-to-elongate tethered system and smaller in a hard-to-elongate tethered system.

In this way, the libration of an easy-to-elongate tethered system diverges, and that of a hard-to-elongate tethered system converges on the periodic solution.

6. Conclusion

The stability of libration of a tethered system is analyzed numerically. Equations of motion of a simplified 3-DOF model, which include in-plane/out-of-plane libration and longitudinal elongation, are formulated through Lagrange formulation without linearization.

Fundamental characteristics of the tethered system are investigated through the periodic solutions and their stability analyzed by applying the shooting method. The effects of system parameters on stability are analyzed, and it is shown that the larger mass of the subsatellite, the smaller cross-sectional area, and the longer tether (easy-to-elongate tether) destabilize libration of the tethered system, and vice versa. It is also shown that drag area, drag coefficient, and orbital altitude and eccentricity determine the rapidity of convergence or divergence. Direct numerical simulations of exact nonlinear equations show the validity of the stability analyses.

Physical interpretation of convergence or divergence of libration is clarified through a comparison with the states of periodic solutions.

Acknowledgments

The authors would like to acknowledge Professors K. I. Oyama and K. Higuchi of the Institute of Space and Astronautical Science for their helpful discussions.

References

1) Oyama, K. I., Sasaki, S., Su, Y. and Balan, N. : Feasibility Study on a Tethered Satellite System, *Proc. of 2nd International Workshop on the Application of Tethered Systems in Space*, ISAS, May 1994, pp. 325–334.
2) Takeichi, N., Natori, M. C., Okuizumi, N. and Higuchi, K. : Dynamic Behaviour of a Tethered System with Multi-Sub-Satellite in Elliptic Orbits, AIAA-2000-1776, AIAA Dynamics Specialists Conference, Atlanta, Georgia, 2000.
3) Modi, V. J. and Brereton, R. C. : Periodic Solutions Associated with the Gravity-Gradient-Oriented System : Part I. Analytical and Numerical Determination, *AIAA J.*, **7** (1969), pp. 1217–1225.
4) Modi, V. J. and Brereton, R. C. : Periodic Solutions Associated with the Gravity-Gradient-Oriented System : Part II. Stability Analysis, *AIAA J.*, **7** (1969), pp. 1465–1468.
5) Karasopoulos, H. A. and Richardson, D. L. : Chaos in the Pitch Equation of Motion for the Gravity-Gradient Satellite, AIAA-92-4369, AIAA/AAS Astrodynamics Conference, Hilton Head, 1992.
6) Karasopoulos, H. A. and Richardson, D. L. : Numerical Investigation of Chaos in the Attitude motion of a Gravity-Gradient Satellite, AAS 93-581, AIAA/AAS Astrodynamics Conference, Victoria, Canada, 1993.
7) Nixon, M. S. and Misra, A. K. : Nonlinear Dynamics of Two-Body Tethered Satellite Systems, AAS 93-731, AIAA/AAS Astrodynamics Conference, Victoria, Canada, 1993.
8) Fujii, H. A. and Ichiki, W. : Nonlinear Dynamics of the Tethered System in the Station Keeping Phase, *J. Guid. Control Dyn.*, **20** (1997), pp. 403–406.
9) Beletskii, V. V. and Levin, E. M. : Dynamics of the Orbital Cable System, *Acta Astronautica*, **12** (1985), pp. 285–291.
10) Onoda, J. and Watanabe, N. : Tethered Satellite Swinging from Atmospheric Gradient, *J. Guid., Control Dyn.*, **11** (1988), pp. 477–479.
11) de Matteis, G. and de Socio, L. M. : Dynamics of a Tethered Satellite Subjected to Aerodynamic Forces, *J. Guid. Control Dyn.*, **14** (1991), pp. 1129–1135.
12) de Matteis, G. : Dynamics of a Tethered Satellite in Elliptic, Non-Equatorial Orbits, *J. Guid. Control Dyn.*, **15** (1992), pp. 621–626.
13) Parker, T. S. and Chua, L. O. : *Practical Numerical Algorithms for Chaotic Systems*, Springer-Verlag, New York, 1989.
14) U.S. Standard Atmosphere, U.S. Government Printing Office, Washington, D.C., 1976.